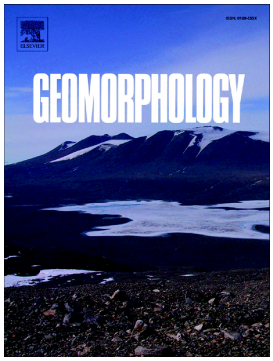

Application of marine radar to monitoring seasonal and event-based changes in intertidal morphology

Cai O. Bird, Paul S. Bell, Andrew J. Plater

PII: S0169-555X(16)30649-3
DOI: doi: 10.1016/j.geomorph.2017.02.002
Reference: GEOMOR 5918

To appear in: *Geomorphology*

Received date: 23 July 2016
Revised date: 7 February 2017
Accepted date: 7 February 2017

Please cite this article as: Cai O. Bird, Paul S. Bell, Andrew J. Plater , Application of marine radar to monitoring seasonal and event-based changes in intertidal morphology. The address for the corresponding author was captured as affiliation for all authors. Please check if appropriate. Geomor(2017), doi: 10.1016/j.geomorph.2017.02.002

Application of marine radar to monitoring seasonal and event-based changes in intertidal morphology

Cai O. Bird, [ab]* Paul S. Bell, [a] Andrew J. Plater, [c]

[a] National Oceanography Centre, Liverpool, UK

[b] Marlan Maritime Technologies Ltd. Liverpool, UK

[c] University of Liverpool, School of Environmental Science, UK

***Corresponding author**: Cai O. Bird

Email address: caibird@noc.ac.uk

Present address: National Oceanography Centre

Joseph Proudman Building

6 Brownlow Street

Liverpool

L3 5DA

United Kingdom

Abstract

This paper demonstrates the application of marine radar and a newly developed waterline mapping technique to the continued surveillance and monitoring of inter- and intra-annual intertidal morphological change, thus capturing new detail on coastal system behaviours. Marine radar data from 2006-2009 are used to create a sequence of waterline elevation surveys that show clear morphological evolution of two different sites in the Dee estuary, UK. An estimate of volumetric change was made at two locations: West Hoyle sandbank and the NW Wirral beach. Both sites exhibited a similar cyclic pattern of volumetric change, with lowest volumes in autumn and winter, respectively. The average beach elevations above Admiralty Chart Datum clearly reflect the observed change in sediment volume, with reduced elevations in winter and increased elevations in summer, suggesting a trend of high-energy storm waves in autumn and winter that remove sediment and simultaneously moderate the vertical dimension of bedforms in the intertidal area. Data at this temporal and spatial scale are not easily obtainable by other current

remote sensing techniques. The use of marine radar as a tool for quantifying coastal change over seasonal and event timescales in complex hydrodynamic settings is illustrated. Specifically, its unique application to monitoring areas with dynamic morphology or that are vulnerable to erosion and/or degradation by storm events is exemplified.

Keywords: **remote sensing; marine radar; intertidal morphology; coastal monitoring; coastal survey**

1. Introduction

1.1. Research context and aims

The coast is temporally and spatially dynamic, with the constant action of waves, wind, currents and tides serving to reshape its physical nature over relatively short geological timescales (Mason et al., 2010). The processes and impacts of morphological change across a gamut of spatial and temporal scales have been studied extensively, and many are well documented (Wright and Short, 1984; Cowell and Thom, 1994). Several examples of these studies include sandy beach (e.g., Johnson et al., 2014; Senechal et al., 2015) and gravel beach response to storms (e.g., Ruiz de Alegria-Arzaburu and Masselink, 2010) in addition to long term, extensive area studies of coastal morphological response to natural and anthropogenic forcing (e.g., Hapke et al., 2010). Changes in the physical environment often have considerable consequences for human populations and biota in close proximity to the coastline. The density and concentration of human population and infrastructure assets are increasing continuously (Nicholls et al., 2011). Additionally, resources in these areas are finite and in many places at risk of degradation and overuse. It is vital, therefore, that the overall health and stability of these increasingly vulnerable areas are monitored, along with their morphological response to further human development and natural processes including storm events (Tătui et al., 2014; Castelle et al., 2015; Dissanayake et al., 2015). The research presented here aims to better capture and understand the morphological behaviours of the estuary-beach interface over a multiple season timescale and to examine the sensitivity and recovery of the associated intertidal beach in response to storms. The purpose of this paper is to

demonstrate how recent advances in radar-based monitoring techniques can be applied to better constrain coastal system behaviours resulting from complex geomorphic interactions in time and space. The resulting data sets provide an effective evidence base for the prediction and tracking of coastal morphological changes in response to a variety of forcings.

1.2. Modelling and monitoring for assessing the vulnerability of coastal areas

Traditionally, coastal defence construction has focused on damage mitigation and protection of vulnerable, high value assets and infrastructure (including extensive residential areas) from flooding and coastal erosion through extensive hard engineering. Examples of these structures negatively affecting the coast and causing increased erosion or undesirable sediment accretion (Kraus, 1988; Gillie, 1997; Phillips and Jones, 2006; Ilic et al., 2007) are numerous, and such developments can act as barriers to natural shoreline adjustments (Dugan et al., 2008; Berry et al., 2014) thus causing intertidal zones to be squeezed out (Doody, 2004; De Vriend et al., 2011). Soft engineering approaches and working with natural processes (European Commission, 1999; McKenna et al., 2008) maintain coastlines through the monitoring and nurturing of dune systems, saltmarshes, tidal flats (Arkema et al., 2013), and dissipative beaches through recharge and nourishment schemes (Hanson et al., 2002; Stive et al., 2013; Wengrove and Henriquez, 2013). Continued pressure on the coastline from erosion and sealevel rise (Wahl et al., 2011; Hanley et al., 2014; Kirshen et al., 2014; Wadey et al., 2014) demands that the response of natural and ‘engineered’ coastal morphological systems to changing forcing factors is modelled and monitored effectively over appropriate timescales.

Coastal engineers and managers often depend on the results of modelling efforts for projecting shoreline response. However, conceptualizing and modelling changes in coastal morphology is particularly challenging over mesoscale (decadal) timescales that lie between the dynamic instantaneous, short-term process and the long-term coastal evolutionary dynamics (Clarke et al., 2014; French et al., 2015; Payo

et al., 2015; van Maanen et al., 2015). Nearshore topographic-bathymetric data are required to drive and validate models used at the foreshore, for example, coastal hydrodynamic and morphological models such as Xbeach (Roelvink et al., 2009) and Xbeach-G (Masselink et al., 2014) are capable of modelling sediment transport (McCall et al., 2015) in addition to profile response.

In addition to modelling, various methods of in situ and remote sensing are utilised to monitor the nearshore zone. Remote sensing techniques are increasing in popularitiy because of their many advatanges over insitu methods (Holman and Haller, 2013)**.** Synthetic Aperture Radar (SAR) and multispectral and optical satellite images can be used to map coastal change on large scales using sequential images and tidal models (Koopmans and Wang, 1994; Mason et al., 1995, 1999; Annan, 2001; Mason and Garg, 2001; Ryu et al., 2002, 2008; Heygster et al., 2010; Liu et al., 2013). Site-specific survey platforms include manual DGPS and TLS surveys (Blenkinsopp et al., 2010; Brodie et al., 2012; Almeida et al., 2013; Almeida et al., 2015) and, more recently UAV/drone systems (Mancini et al., 2013; Rovere et al., 2014). Video camera analysis is widely used in the observation of nearshore processes, including the derivation of hydrodynamics and topography (Holman and Guza, 1984; Holman et al., 1993; Holland et al., 1997; Aarninkhof et al., 2003, 2005; Davidson et al., 2007; Holman and Stanley, 2007; Uunk et al., 2010; Sobral et al., 2013; Santiago et al., 2013); and infrared cameras are able to operate in low light conditions to observe hydrodynamics in the nearshore zone (Jessup et al., 1997; Watanabe and Mori, 1997).

Standard marine navigation radar can be used to create image data appropriate for use in coastal monitoring. The fine spatial resolution (3-10 m depending on range setting) and unique interaction between radar-emitted EM waves and a rough sea surface (Valenzuela, 1978) allow numerous critical nearshore hydrodynamic phenomena to be observed and measured. Marine radar is ideally suited to observing wave fields and has been used extensively to derive wave spectra (Reichert et al., 1999; Nieto-Borge and Guedes Soares, 2000) based on techniques pioneered by Young et al. (1985). There are a

number of approaches to determining and filtering these wave spectra to extract wave and current statistics (Nieto-Borge et al., 2004, 2008; Senet et al., 2001, 2008; Hessner et al., 2008; Serafino et al., 2010, 2012). In this respect, Bell et al. (2012) successfully determined and mapped surface currents around the island of Eday off the north-eastern coast of Scotland. Subtidal water depths can also be estimated based on the observed wave behaviour, which allows nearshore bathymetric maps to be created (Bell, 1999, 2006, 2008; Flampouris et al., 2009; Bell and Osler, 2011). Previous researchers have mapped shoreline positions using marine radar by imaging the waterline in the spatial domain and describing beach contour levels using time-stamped time exposure images and a record of tidal elevation (e.g., Takewaka, 2005). This technique was also used to observe morphological change at a river mouth (Takewaka et al., 2009). The ability to robustly map intertidal zone elevations on a pixel-by-pixel basis without the need to consistently observe wave fields (Bell et al., 2016) adds to the capability of marine radar in coastal monitoring. This paper expands on previous research by demonstrating its application to monitoring changing intertidal morphology over the multiseasonal timescale.

2. Methodology

2.1. Data collection and study site description

Data used in this contribution were gathered for the *Liverpool Bay Coastal Observatory* over 2005-2009 (Bell, 2008) using a *Kelvin Hughes* marine radar operating at X-band, 9.4 GHz located in an elevated position (~25 m aMSL) on Hilbre Island, at the mouth of the Dee estuary, UK (Fig. 1). The radar waterline survey method used to generate results shown in this paper will be briefly described in the following section along with a description of its application to the observation of seasonal trends in morphology along the Wirral coastline and within the sandbanks of the Dee estuary.

The morphology of the Dee and nearby Mersey estuaries have changed significantly over the last few centuries (e.g., Marker, 1967), and regular dredging is required to maintain the deepwater navigation

channel that cuts through Salisbury Bank to the southwest into Mostyn port and out into the Irish Sea via the Welsh Channel or 'Wild Road' as it is known locally.

The Dee estuary exhibits flood-dominated tidal asymmetry and is a mature, infilled estuary approaching morphological equilibrium (Moore et al., 2009)**.** The Dee has long been a sediment sink and has experienced continued expansion of saltmarsh since at least 1900 (cf. Rahman and Plater, 2014). In addition, mobile sedimentary bedforms within the outer estuary and mouth may still be encroaching on channels and tidal inlets, with the potential to cause a navigation hazard (e.g., Demirbilek and Sargent, 1999) and change the topographical distribution of the estuary significantly. This is of particular concern within the Dee estuary where critical wing components for the Airbus A380 'Superjumbo' passenger jet are ferried to Mostyn port before being shipped to mainland Europe for final assembly.

Hydrodynamics in the Dee estuary are extremely varied; waves in the eastern Irish Sea are fetch limited with significant wave heights of < 5.5 m and mean periods of < 8 s. However, the very high tidal range of more than 10 m on high spring tides exposes a large expanse of intertidal area that is influenced by the actions of waves and tides across an area of several square kilometres at low tide in the estuary mouth. More detailed analysis of the Dee estuary and Liverpool Bay hydrodynamics can be found in Bolaños and Souza (2010), Bolaños et al. (2011), Wolf et al. (2011), and in Thomas et al. (2002) for an assessment of historical morphological change and resulting hydrodynamic regime change.

2.2. Radar-based intertidal topographical survey methodology

Marine radar 'snapshot' images (generated every 2.4 s) are temporally averaged over 10 min, creating a series of time exposure images (Fig. 2) taken every hour throughout 2006-2008. These images are analysed in 2-week blocks such that the full spring-neap period is observed.

When these images are viewed in sequence, the spatial location of the waterline can clearly be seen migrating across the image space according to the rise and fall of the tide. The higher pixel intensity results from greater amounts of microwave energy being reflected from the breaking waves in the surf zone. Surface roughness, and therefore image pixel intensity, is determined by wind speed (Valenzuela, 1978), direction (Dankert et al., 2003; Dankert and Horstman, 2006), and wave heights and is also influenced by convergent currents on the ebb and flood tides channelled by submerged sandwaves, sandbanks, and tidal flats farther out in the estuary (Alpers, 1984).

By extracting a given image pixel intensity at each time step over a 2-week period, the temporal signal of a spatially transgressing waterline can be obtained with a time series of intensities showing clear transitions between high and low intensity, representing a state transition from wet to dry at each pixel. The temporal gradient of this time series gives a sequence of pulses, the peaks of which indicate the time at which a pixel transitions from wet to dry (Bell et al., 2016). Each tidal elevation within a given tidal range, 0-10 m with 10-cm vertical resolution in this case, also has a unique temporal signal indicating the times of transition from wet to dry at a given location according to the tidal cycle.

The signal of pixel intensity gradients from every point in the input image sequence is matched to a tidal elevation above Admiralty Chart Datum (ACD) using the temporal waterline method detailed in Bell et al. (2016) in which examples of this procedure are demonstrated. Figure 3 shows a simple schematic of the technique used to derive intertidal elevations.

The resulting maps show the mean elevation of the radar-observed waterline over the 2-week analysis period, giving a good approximation of the intertidal morphology at that time. The algorithm can make use of data collected over a shorter time period; however, the full tidal range between a given spring and neap tide will not be observed. Elevations outside of the tidal range are unable to be resolved given the lack of

tidally driven waterline transitions. The maps are filtered according to correlation coefficient derived by the waterline matching algorithm, with low correlations representing areas of low confidence in the accuracy of the derived elevations (Bell et al., 2016). Typically these zones reflect areas that are shadowed from the radar antenna or that are subtidal zones where no cycle of tidal wetting and drying is detected. In situations where a radar is deployed for extended periods of time, continued data collection permits the generation of repeated surveys, allowing morphological changes in an area to be monitored.

It is possible to improve the estimations of elevations by temporally filtering the resulting sequence of elevation results at each pixel location. A robust smoothing algorithm (Garcia, 2010) that is weighted by the signal of maximum correlation coefficients corresponding to each elevation result is applied to each pixel record of radar-derived elevations. Thus, outlying data and missing values that have low correlation coefficients are less able to negatively influence the smoothed elevations. This enables missing data to be filled with an approximate elevation whilst still retaining the overall trend of the signal, giving an unbroken record of elevations over long time periods that allows for the evolution of a given intertidal area to be tracked effectively. Results of applying this smoothing to a smaller data set can be seen in Bell et al. (2016). The issue of filling missing data in data sets used to monitor coastal morphology was also addressed by Holman et al. (2013) where hourly bathymetric surveys generated using the cBathy algorithm applied to video camera data often had gaps caused by poor lighting conditions. Gaps were filled using a robust Kalman filtering technique and resulted in derived elevations showing an RMS of 0.51 m when camera-derived elevations were compared with a bathymetric survey. The authors decided not to apply this type of Kalman filtering to the radar surveys at this time because of the desire to weight the smoothing strictly by correlation coefficients and the much lower sampling frequency of the 2-weekly radar surveys when compared to hourly camera-derived surveys.

3. Results

Figure 4 shows the results of two weeks of radar data (26 March 2006–8 April 2006) analysed using the radar temporal waterline method, with the polar radar data projected onto a Cartesian grid with 5-m spatial resolution. The noise in this plot at longer ranges (marked by black rings in Fig. 4) is indicative of the increased area lying in shadow and the drop off in back-scattered radar power, resulting in lower intensities and more unstable pixel signals at longer ranges. Figure 4 is colour-coded according to waterline elevation above ACD and illustrates two sites: site A is the West Hoyle sandbank and B is a section of the NW Wirral beach, the morphology of these areas will be examined in more detail in the following sections. Site A is an interestuary sandbank, isolated at low tide from the beach and from the north Wirral coastline to the east and the north Wales coast to the west. Site B on the other hand is a beach location that is connected to the north Wirral shore. Because of the dynamic estuarine morphology in the Dee, levels of exposure to wave action and storm events are likely to vary greatly across the estuary and between these sites.

Accuracy and stability levels of this technique have been assessed in some detail in Bell et al. (2016) by comparison with an aerial LiDAR flight taking place at the same time (early October 2006) as the radar survey. Importantly, the LiDAR represents a snapshot of elevations; while the radar method estimates the mean elevation over a 2-week period, thus there will be some variation in results. Analysis of changing elevations at several fixed rock locations around Hilbre Island showed deviations of ±10 cm over a 10-month testing period, suggesting that elevation changes observed by the radar across the study area reflect actual changes in morphology. Accuracy was found to vary with range from the radar, with RMSE of 31 cm and bias of 12 cm within the first 750 m. Larger average error is observed as range increases (indicative of increased area subject to shadowing and lower radar returns at longer ranges) from RMSE of 61–83 cm and bias of 48 to 59 cm across the remaining range extent (Bell et al., 2016).

This radar survey technique has some limitations. The total area shadowed from the radar is influenced by a combination of the height of the radar antenna, the height of observed bedforms and their ranges from the radar, and the surrounding ground topography, e.g., hills, cliffs, or buildings that may obscure vision in the alongshore directions. Consequently, careful consideration must be given to the siting of the initial radar deployment, especially as the radar must remain stationary during data collection. Areas with a very small tidal range, narrow intertidal area and/or a very steep beachface would likely not present ideal conditions for the application of this methodology. The technique also requires an accurate record of tidal elevations in order to estimate elevations; robust methods of retrieving tidal elevations in remote areas are currently under development to compliment the radar survey technique.

A waterline survey in the form of Fig. 4 was completed for every two-week period from the beginning of 2006 to the end of 2008, using a total of 256 images for each analysis period. However, during some periods, surveys could not be produced as a result of failures of radar hardware, software, or in the remote power supply; these gaps in the dataset are detailed in Table 1.

2006		2007		2008	
Month	**Day**	**Month**	**Day**	**Month**	**Day**
1	1	1	1	1	15
1	14	1	13	1	29
1	28	1	27	2	9
2	12	2	10	2	23
2	26	2	24	3	7

3	11	3	10	3	21
3	25	3	24	4	4
4	8	4	7	4	18
4	22	4	21	5	6
5	6	5	5	5	20
5	20	5	19	6	5
6	3	6	2	6	19
6	17	6	16	7	1
7	1	6	30	7	12
7	15	7	14	7	26
7	29	7	28	8	9
8	12	8	11	8	23
8	26	8	25	9	7
9	9	9	15	9	21
9	23	9	29	10	4
10	7	10	13	10	18

10	21	10	27	11	1
11	4	11	15	11	15
11	18	11	29	11	29
12	2	12	13	12	13
12	16	12	27	12	27

Table 1

Documented dates of completed surveys and missing data throughout the 3-year deployment at Hilbre Island, grey highlighted dates indicate missing data

3.1. Accuracy of radar-derived elevations at site A (West Hoyle sand bank).

Site A, the location of which is shown in Fig 4, is a section of the West Hoyle sandbank. Bedforms across this feature are known from local anecdotal evidence to be highly mobile. Figure 5A shows this area cropped out of the radar waterline data, and Fig. 5A shows the same area extracted from a LiDAR survey flown at the same time period (October 2006).

The overall accuracy of this technique has been explored in some depth in Bell et al. (2016): however re-examining this aspect for West Hoyle sandbank gives greater context to these results. The differences between radar-derived elevations and the LiDAR elevations must be set in context with regard to the different physical phenomena being observed, that being the absolute bed elevation directly measured by the LiDAR and the water surface level being imaged by the radar and used to indirectly estimate bed elevation. Figure 5C shows the residual differences between the radar waterline elevations and the

LiDAR bed elevation measurements, in which the majority of the area of West Hoyle sandbank is well defined with elevation differences of 0–50 cm (green and yellow areas) with two main concentrations of larger differences >50 cm around the shallower areas of the sandbank. Potential sources of this error are discussed below.

Figure 5D shows the areas shadowed from line of sight of the radar by intervening topography and shows that line of sight to most of the survey area is relatively unobstructed from the radar antenna and therefore shadowing is not likely the cause of the larger elevation differences that can occur in areas not shadowed. The issue of pooling water could be a contributing factor to the overestimation of elevations (Bell et al., 2016). During the ebb tide, water is retained in these channels for longer periods than on the slopes of sandbanks, especially if water is draining from upstream. The radar continues to image this water surface even as the recorded tidal elevation falls until it drains completely, shifting the times at which the radar detects a transition from wet to dry and causing elevations to be overestimated. This phenomenon is potentially contributing to the general overestimation of elevations across the surveyed area as water slowly drains off the shallow sandbank. In addition, these channels are likely more sheltered from the wind, which potentially reduces the ability of the radar to detect the waterline transitions in these areas during periods of low sea state (when low winds do not roughen the sea surface sufficiently to allow radar detection). Changes in pixel intensities within these areas are still tidally driven, often resulting in a high correlation coefficient in the elevation-matching algorithm. This means that current methods of quality control do not automatically filter regions subject to tidal pooling/draining and further work must be done to highlight these areas.

Figure 6 shows a comparison between the radar and LiDAR elevations at site A, taken during October 2006. This figure highlights the overestimation of elevations by the radar technique. The authors believe that these systematic errors in elevation are likely to be a result of a combination of physical effects including but not limited to

(i) slight differences between the nominal still water line (tidal elevation) and the location of the shore break as imaged by the radar (Bell et al., 2016);

(ii) wave setup and runup shifting the breaker line onshore relative to the still water line;

(iii) pooling of water as it drains over very shallow (1:100–1:200 slope) intertidal areas causing shifts in waterline transitions;

(iv) localised currents induced by the mass of water conveyed shoreward by breaking waves draining back off the beach — This could cause a shift in the location of the shore break similar to (i); and

(v) the assumption of a uniform, instantaneous tidal elevation across the analysis domain being an oversimplification.

The overestimate illustrated in Fig. 6 suggests that (i) is the most likely and significant physical effect causing the errors, although a combination of factors is involved. At any particular location the errors appears to result in a relatively stable offset, a fact that was verified by the observation of waterline-derived elevations of fixed rock targets in Bell et al. (2016). Thus the determination of absolute elevations will include some degree of error, but the observation of changes in beach morphology may be conducted with some confidence. A more detailed study of the contribution of these various physical effects to the absolute errors will be the topic of further work.

The following sections illustrate changes in the inferred morphology of West Hoyle sandbank (site A) and a large area of NW Wirral beach face (site B) from March 2006 to December 2008.

3.2. Monitoring morphological change in intertidal areas

In order to explore changes in intertidal morphology, several sites have been chosen to highlight the spatial variability over a relatively small area. The study area in the Dee estuary is heterogeneous; with

extensive shallow sandy beaches to the northeast of Hilbre Island, sandbanks to the west, mixed mud and sand intertidal flats to the east, and saltmarsh to the southeast, along with several rocky outcroppings. The radar survey technique derives elevations well over all of these environments, suggesting wide applicability to other diverse sites.

The radar survey technique provides the ability to estimate changing sediment volumes across large areas of the survey environment. An estimate of sediment volume (relative to Admiralty Chart Datum) was made at each grid location and the mean total volume per pixel at the West Hoyle sandbank and the NW Wirral beach calculated every two weeks. Figure 7A shows the estimated sediment volume over nearly three years at West Hoyle sandbank (site A), with the winter seasons (December-February) marked as dashed red lines and gaps in the data set being filled using a third-degree polynomial. Figure 7B shows volumetric data from the NW Wirral beach (site B). Wave data from the Liverpool Bay waverider buoy (WMO ID: 62287, operated as part of the *CEFAS wavenet* in the Irish Sea off the coast of the Wirral Peninsula) provided high temporal resolution (every 30 min) measurements of significant wave heights from 2006 to 2009 while the radar was deployed. The buoy was located at 53°32'.01N, 003°21'.31W. Significant wave heights, periods, and dominant directions from January 2006 to December 2008 are shown in Fig 7C.

The Dee estuary is currently at or approaching stability at the equilibrium stage of its morphological evolution (Moore et al., 2009). Figures 7A and 7B broadly confirm that there is little net change over the analysis time period, but with deviations over the course of a year, this does suggest a dynamic equilibrium state where the Dee estuarine system is constantly adapting to new boundary conditions and forcings (e.g., Van Dongeren and De Vriend, 1994). The signal of changing sediment volume at site A (Fig. 7A) indicates lowest volumes towards the ends of the autumn season and early winter. There is a significant temporal lag between the two sites, and it may be that material is being transported from elsewhere in the local domain such as the outer areas of the East and West Hoyle sandbanks or the

Point of Ayr to the west. Maximum sediment volumes are seen in spring and summer when wave conditions are generally calmer (see Fig. 7C). This seasonal cycle of changing volume is reflected well in the cycle of changing elevations shown later in Fig. 11, suggesting a removal of material and a flattening of bedforms during autumn and winter. One of the authors who visited the site before and after an autumn storm in September 2007 also observed this effect. Well-defined bedforms of height 0.5-1 m and wavelength in the order of 100 m were present before the storm but were almost completely flattened afterward.

Site B follows a similar pattern to that of site A in terms of changing sediment volumes, as shown in 7B. The key difference here, however, is that lowest sediment levels are seen in mid-winter. This lag in material loss could be indicative of changing wave angle and climate affecting the different locations in different ways or potentially some transfer of material from one site to the other. The record of daily averaged significant wave heights throughout 2006-2009 show that wave heights are generally high in autumn and winter, this is also reflected in the monthly averaged significant wave height values (red line in Fig. 7C). This suggests that the seasonal cyclicity in sediment volume flux is influenced by the change in wave climate as well as the underlying tidal cyclicity throughout the year. The extent to which the changing wave climate influences the two sites analysed clearly varies significantly given the lag time in volume change.

3.3. Observing intertidal bedforms and changing beach elevations

At the temporal resolution outlined in Table 1, changes in the morphology of West Hoyle sandbank can be seen clearly. Figure 8 shows a sequence of radar waterline elevations described using two weeks of data at a time and a sample survey was extracted every five months to illustrate changes in morphology across the sandbank. The movement of mesoscale bedforms can be seen across the sandbank and is representative of the sediment translation evident in Fig. 7. This movement is evidenced effectively in the

video attached in supplementary material, *WestHoyleBank_MorphologicalChange.mp4*, which makes use of all available two-week surveys across the three-year deployment and presents this information as a series of surface plots with a 25x vertical exaggeration to emphasize morphological features. While the accuracy of several regions described in Fig. 5 is relatively low when compared to LiDAR data, Fig 8 and the supplementary video show that the observed over-estimations are relatively consistent between surveys, and that indications of relative changes in morphology are captured despite the lower absolute accuracy of this iteration of the radar-based survey.

Site B comprises the intertidal flats area immediately to the east of Hilbre Island where the radar is situated (Fig. 4). A similar exercise as that applied to site A was performed in order to observe the changing beach elevations at this site. The accuracy of results from this area compared to LiDAR elevations was explored in detail in Bell et al. (2016) and are not reiterated here. Significantly, shadowing is more of an issue where there are many quasi-linear tidal channels and bedforms that give rise to a complex local morphology.

Figure 9 shows a series of plots constructed using radar waterline elevation data illustrating the migration of linear sedimentary bedforms with wavelengths of the order of 200 m; these appears to be subtidal to intertidal bars that weld onto the beach during late 2007/early 2008. These plots are extracted from the three-year time series every five months in the interest of demonstrating this phenomenon. The reader is also directed to the online supplementary material where a video showing the changing morphology as a sequential display of surface plots, *EasternFlats_MorphologicalChange.mp4*, is available.

Figure 10 shows the total residual change in waterline elevation between the start (March 2006) and the end (December 2008) of the three-year survey period, with the red regions indicating erosion and the blue areas indicating accretion. The northern section of the sandbank has experienced significant loss in elevation (~1 m); while the southern, central, and western sections of the bank have accreted. This is

consistent with known behaviour at the site, as there is a navigation marker buoy located at the far eastern edge of the sandbank that is periodically moved to the south by the local harbour authority throughout the duration of the monitoring period.

Estimations of sediment volume are not the only measure of beach state and shoreline health able to be resolved with this method. The variation of mean elevations of a given region gives an intuitive overview of the beach profile condition, higher mean elevations can indicate the presence of significant bedforms or a more uniform overall accretion, while lower elevations reflect a 'flattening' of bedforms or their migration out of the study area. The pattern of these mean elevations is similar to those of the total sediment volume change over the three years. Figure 11 illustrates the change in mean waterline elevation (m) at site A at each available two-week period from March 2006 to December 2008, as well as their deviation around the mean beach elevation (purple solid line). The red line describes 2006 elevations, the green line 2007, and the blue 2008. Figure 11 clearly shows that all lines follow a similar pattern where the sandbank elevations rise above the mean elevation in summer and drop below this in winter.

Figure 11B illustrates the change in mean waterline elevation at site B, reflecting the changing sediment volume relatively well with elevations below the three-year average in winter and above in summer. Loss of material begins around one month later than at site A but seems to follow a similar pattern, suggesting a progressive change in intertidal morphology across the estuary is driven by seasonal variations in hydrodynamic forcing.

3.4. Radar-derived cross-shore profiles

Beach profiles are an important form of input data to many nearshore morphological and hydrodynamic models, for example XBeach and XBeach-G (Roelvink et al., 2009; Masselink et al., 2014). Traditional

methods of measuring beach profile evolution over time often involves the repeated sampling of a series of cross-shore profiles and measuring the differentials to determine erosion or accretion and track migration of observed bedforms (Pye and Smith, 1988). The radar waterline technique allows the user to extract multiple profiles from a desired location and analyse their evolution over a long period of time, allowing variations due to bedform crests and troughs to be removed, resulting in a mean barless beach profile such as used by Ruessink et al., (2002). Profiles can also be extracted for use in further processing or as model input.

Figure 12A shows an area of the intertidal flats to the east of Hilbre Island that was extracted in order to sample several cross-shore profiles to demonstrate changes in these profiles over three years. Figure12B shows this area rotated, such that each row in the matrix is a cross-shore profile and each column is an alongshore profile. The locations of four transects (T1-4) are also shown. The accuracy of these profiles when compared to LiDAR data was examined in Bell et al. (2016).

In order to examine changes in beach profile elevation throughout the three-year study period, these transects were arranged into timestacks shown in Fig. 13, with time on the *y*-axis, cross-shore distance on the *x*-axis, and elevation from ACD on the *z*-axis. The migration of these sedimentary features is seen clearly in Fig. 13, particularly the linear migration of a bedform crest that is evident in transect 2. Two clear crests are present in early 2006 and their progression in a shoreward direction captured. During winter 2007 these crests are clearly flattened to some extent. In the spring season the bedforms build up again and resume shoreward migration before appearing to weld onto the beach during 2008. A clear cyclicity to the erosion and accretion can be observed across these transects that is most evident in transects 3 and 4 demonstrating erosion of the upper, shoreward regions of the profiles during autumn and winter and subsequent accretion in the summer. This seems to support trends in sedimentary volume and elevation seen in earlier sections. The absence of linear bedform crests in transects 3 and 4 could be a result of their sheltered situation in lee of Hilbre Island reducing their exposure to wave action. Mean

wave energy density figures are also calculated using data from the CEFAS Wavenet offshore buoy (details given above). These values are derived from the mean significant wave height over each 2-week period corresponding to those of radar data collection. Periods of highest wave energy density correspond to times of greatest erosion on the cross-shore profiles.

3.5. Morphological response to storm events

In addition to long-term observations and snapshot surveys, this method can also be tuned to selectively survey waterline elevations over a given area leading up to and immediately following a storm event. Directly monitoring post-storm recovery is a difficult task with insitu surveys because of the necessity to track synoptic weather data and predictions. In contrast, continuous monitoring by a radar system potentially allows automation of pre- and post-storm surveys. The storm *Britta* in late October (29th) to early November (4th) 2006 was primarily a North Sea storm and contributed to gusts in the region of 170 km/h in many coastal areas across western Europe including Denmark, Norway, and Scotland. As waves in the Irish Sea are predominantly fetch-limited (Dissanayake et al., 2015) it is assumed that similar (albeit much less dramatic) storm conditions contributed to the generation of the waves being measured by this buoy during this period.

Radar data were processed for two weeks up until 29 October 2006 when significant wave heights began to increase up to a local maximum daily mean of 2.4 m. Peak significant wave height over the storm period was 3.4 m, and peak wave period of 9 s were observed on 31 October 2006 at 08:00. A survey was generated for this pre-storm period and another for the following two weeks. Figure 14 shows the residuals between the survey before and following storm *Britta* around Hilbre Island. Red areas indicate erosion, with maximum values suggesting around 1 m of relative (as the results indicate waterline elevations) sediment loss from the crests of bedforms.

A visual comparison between Fig. 14 A and 14B shows a clear overall reduction of elevation across the beach. Numerous linear features of erosion can be seen running from southwest to northeast along the beachface; these are likely the crests of bedforms being flattened or being redistributed farther offshore (as indicated by the areas of accretion indicated in blue concentrated close to the subtidal margins). The extracted subimage marked by the black boundaries shows residual elevation change (see Fig. 14C) between the pre- and post-storm radar surveys.

4. Discussion

The application of the radar waterline method developed by Bell et al. (2016) to the problem of intertidal morphological monitoring has been investigated in this contribution. Several sites within the intertidal area of the Dee estuary, northwest UK were selected in order to explore their change in morphology. Significant changes in waterline (and therefore implied underlying bed elevation) were observed at both sites selected. At site A, West Hoyle sandbank, large dynamic bedforms can be seen migrating across the bank. This is consistent with the theory that the Dee is an estuary approaching overall equilibrium, but with significant variations across an annual cycle in the patterns of local sediment flux, as evidenced in Figures 7A and 7B. The described changes in local sediment levels are driven not only by underlying tidal cyclicity but are also modulated by variations in wave conditions according to broadly seasonal cycles. The time lags in sediment fluxes between the two sites analysed indicate differences in susceptibility to wave action between the two sites, which are likely a result of their different geomorphological characteristics. The NW Wirral beach differs from West Hoyle sandbank in that sandbanks in a more central position in the estuary mouth are likely to be more exposed to waves than the tidal flats adjacent to the beach. In addition, site A has a much shallower cross-shore gradient and a lower maximum elevation: this elevation difference will influence, to some extent, the duration and impact of nearshore processes affecting the area over the course of a given tidal cycle; and the difference in gradient will contribute to the determination of runup extents and wave-breaking processes (Masselink et al., 2006).

Figure 4 illustrates that the upper regions of site B are sheltered by Hilbre Island from westerly waves, potentially reducing erosion of the upper beachface during moderate wave conditions. Waves incoming from the north and northwest are likely to break and their energy will be dissipated during the transition across East Hoyle sandbank to the north of site B.

The differences in mean beach height shown in Fig. 11 also show annual and interannual cyclicity, with differences in mean elevation of ~40 cm between November 2006 and June 2007 at site A and ~30 cm between December 2006 and July 2007 at site B. Although the absolute values of these elevations may not be as accurate as LiDAR surveys, radar-derived elevations were previously shown to be stable from survey to survey (Bell et al., 2016). This gives confidence that the changes in radar-derived elevations do reflect changes in topographic elevation. Further observations of cyclic changes were made by visualising changes in cross-shore transects in Fig.13, and periods of highest wave energy appear to correspond to the autumn/winter seasons of 2007 and 2008 where the beach profile was flattened significantly before restabilising in spring of the following years. Anecdotal evidence from local authorities including the Wirral Borough Council Ranger Service during visits to the study site also indicated substantial changes to localised beach elevations observed by the Ranger Service based on the emergence and disappearance of rocky outcrops beneath the sand within the intertidal area.

A clear disadvantage of relying solely on cross-shore profiles is the lack of three-dimensional monitoring that potentially causes the passage of a bedform to be missed if it migrates between two transects. This can also give the false impression of increased erosion from a transect when it is possibly a case of bedform migration. Many studies seek to address this by taking many profiles closely spaced along an area of the coast and often interpolating between profiles, potentially introducing significant errors (Plant et al., 2002). However, the cost in personnel and time taken increases as more profiles are taken.

The morphological impacts on the intertidal area to the east of Hilbre Island during a storm were observed by the radar. The area highlighted in Fig. 14 shows the flattening of an intertidal bar and the apparent redistribution of material in the seaward direction. However, the temporal resolution of 2 weeks used in this analysis is likely not sufficient to properly quantify the effects of a single storm, in this instance wave heights increase again only a week after the storm, and thus some of the changes recorded may in fact be a result of a separate storm event. Resolving this may be achieved by using fewer data in the analysis (for example only one week before and after the storm event) although results will likely be less accurate, or by using a two-weekly moving window analysis, stepping forward by several days at a time.

Sandbank systems often provide natural coastal defences, serving to dissipate incoming waves and, as such, are often exposed to high-energy events, potentially suffering degradation and erosion (Hanley et al., 2014). Many beach nourishment schemes aim to replenish material lost to erosion, and thus, the presented technique for monitoring intertidal areas could provide a cost-effective and robust option for the long-term assessment of the effectiveness of such schemes.

4.1. Methodological improvements and further work

The methodology presented shows itself to be aptly suited to long-term coastal morphological monitoring. Significant improvements are planned through several key development efforts, the first of which is an increase in the temporal resolution of the input time-exposure images. In the present study, data were recorded hourly – limited by data storage available at the time of data collection (2005-2008). As a result of the large tidal range in the Dee estuary, the water level can change significantly within an hour. This could result in certain elevations being omitted from the analysis as the image sequence has insufficient temporal resolution to capture the whole transition of the tidal range. This shortcoming could be alleviated by processing time-exposure images more frequently or even continuously, capturing more of the

waterline progression through the image sequence. This may also assist in the method's application to tracking changes resulting from instantaneous events, such as storms or other wave events.

Further improvement are possible with the application of more advanced image processing and filtering techniques to the basic input image data. The objective of these techniques would be primarily twofold: (i) to reduce over-exposure and excessively high pixel intensities at short ranges (a result of radar power saturation and pulse width also known as the ‘main bang’), (ii) to increase intensities at longer ranges, alleviating radar power drop off. In addition, reducing the noise of sea clutter in the subtidal area would serve to prevent many false waterline elevation acquisitions in these areas. Algorithms to accomplish these aims are currently under development and will be explored in further work.

The differences between the waterline-derived elevations and survey data require further study. Numerical models may provide some insight into the propagation of the tide across the study domain, rather than assuming a uniform tidal elevation across the site. This may also assist in quantifying the slow drainage of water from the sand flats on the ebb of the tide and possible regions of pooling water. The dependence of the location of the shore breaker line relative to the still water level on a range of hydrodynamic effects may also be numerically explored with the assistance of beach profile models such as XBeach.

5. Conclusions

A novel radar waterline survey method is applied to the difficult task of monitoring intertidal morphology over long periods of time. Data were collected using a standard marine radar operating at X-band (9.4 GHz) with a 3.83-km radial range from an installation on a remote island. These data were used to create a series of time-exposure images of an estuarine environment, and the pixel intensities from these images were used as input to a matching algorithm along with a record of tidal elevations in order to

estimate a waterline elevation above chart datum for that individual pixel. Just under three years of data were processed, producing a survey of elevations every 2 weeks (where possible).

Assessments of morphological change exposed the dominant trends of volumetric change at both sites, revealing a trend of sediment loss (Fig. 7) in autumn and winter and subsequent accretion in spring and summer for the sandbank and beach sites, respectively (Fig.11). This potentially indicates overall trends of sediment erosion by means of stronger wave events during winter; these wave events also serve to moderate the vertical dimension of intertidal bedforms. In the summer, wave conditions are more stable (indicated by records of daily significant wave heights from a nearby Waverider buoy shown in Fig. 7C allowing the tides and currents to reestablish clearly defined bedforms and to rework sediment back onto the beaches.

The radar waterline method thus offers a tool for monitoring intertidal morphology over long periods of time and across large areas. While vertical differences compared to a LiDAR system are currently up to several decimetres, these differences appear to be relatively consistent at any particular location. Thus, the high temporal resolution of the radar survey technique allows repeat surveys to quantify morphological change over large areas. This also potentially allows the technique to be applied to the tracking and measurement of sedimentary bedform migration. The elevation estimates provided by the radar survey reflect the mean elevation over two weeks; and with this survey having a 5-m spatial resolution (the resolution of radar-derived surveys varies depending on the antenna and carrier frequency of the radar) the morphological details of some of the smaller bedforms that change on a daily–weekly basis, such as those observed by Anthony et al. (2004), are being smoothed out. These data therefore provide a holistic view of the larger-scale seasonal changes. Limitations imposed by irregular surveying, collection of only two-dimensional profiles, and focussing on surveying only smaller areas have previously prevented the effective observation of seasonal change and bedform migration at this spatial and temporal scale.

In addition to providing data to validate modelling efforts, this methodology can be used to either support other survey techniques in large-scale survey campaigns or act as a stand-alone sensor. The versatile nature of radar image data allows other data processing methods (such as wave inversion analyses to retrieve subtidal bathymetry and surface currents) to be applied to data collected during these deployments. Robust automated collection of wide area intertidal surveys was not previously possible with marine radar and is not possible using other remote sensing techniques at this spatial scale and update rate. The application of this radar-based technique may significantly improve the situational awareness of coastal managers prior to large-scale engineering projects, and provide stakeholders with better long-term information, or analytics (i.e., Coastal Analytics) describing the overall 'health' of a given shoreline as conditions change or as maintenance/coastal defence projects progress.

Acknowledgements

Thanks are extended to many organizations and individuals for their contribution to this work. The authors would like to extend gratitude firstly to the *Centre for Global Eco-Innovation (CGE)* through the *European Regional Development Fund (ERDF)* grant number: X02646PR and *Marlan Maritime Technologies* for funding Cai Bird's PhD studies of which this work is a constituent part. Funding was also provided by *Engineering and Physical Sciences Research Council* for investigator time on the *ARCoES* project EP/1035390/1. The radar data used in this contribution were collected by the *National Oceanography Centre (NOC) Liverpool* under the umbrella of the *Liverpool Bay Coastal Observatory* and was funded by the *UK Natural Environment Research Council* under *National Capability Funding.* Thanks are also given to the Wirral Borough Council Ranger service, specifically the former Hilbre Island Ranger Mr. David Cavanagh who assisted in deployment and maintenance of a remote radar system in a very challenging environment. Finally, the authors are grateful for the efforts of the anonymous reviewers and editor of this journal whose comments and constructive feedback greatly improved this manuscript.

References

Aarninkhof, S.G.J., Turner, I.L., Dronkers, T.D.T., Caljouw, M., Nipius, L., 2003. A video-based technique for mapping intertidal beach bathymetry. Coast. Eng. 49(4), 275–289. DOI:10.1016/S0378-3839(03)00064-4

Aarninkhof, S.G.J., Ruessink, B.G., Roelvink, J.A., 2005. Nearshore subtidal bathymetry from time-exposure video images. J. Geophys. Res. Ocean. 110, 1–13. DOI:10.1029/2004JC002791

Almeida, L.P., Masselink, G., Russell, P.G., Davidson, M., Poate, T., McCall, R., Blenkinsopp, C., Turner, I., 2013. Observations of the swash zone on a gravel beach during a storm using a laser-scanner (Lidar). J. Coast. Res. 1(65), 636. DOI: 10.2112/SI65-108.1

Almeida, L.P., Masselink, G., Russell, P.E., Davidson, M.A., 2015. Observations of gravel beach dynamics during high energy wave conditions using a laser scanner. Geomorphology 228, 15–27. DOI:10.1016/j.geomorph.2014.08.019

Alpers, W., and Hennings, I., 1984. A theory of the imaging mechanism of underwater bottom topography. J. Geophys. Res. 89, 10529-10546.

Annan, J., 2001. Hindcasting Coastal Sea Levels in Morecambe Bay. Estuar. Coast. Shelf Sci. 53, 459–466. DOI:10.1006/ecss.1999.0626

Anthony , E.J., Levoy, F., Monfort, O., 2004. Morphodynamics of intertidal bars on a megatidal beach, Merlimont, Northern France. Marine Geology 208 (73 - 100). DOI: 10.1016/j.margeo.2004.04.022.

Arkema, K. K., Guannel, G., Verutes, G., Wood, S. A., Guerry, A., Ruckelshaus, M., Kareiva, P., Lacayo, M., Silver, J. M., 2013. Coastal habitats shield people and property from sea-level rise and storms. Nature Climate Change 3(10), 913-918. DOI: 10.1038/NCLIMATE1944

Bell, P. S., 1999. Shallow water bathymetry derived from an analysis of X-band marine radar images of waves. Coastal Engineering 37(3), 513-527. DOI:10.1016/S0378-3839(99)00041-1

Bell, P. S., 2008. Mapping shallow water coastal areas using a standard marine X-Band radar. In: Hydro8, Liverpool, 4th-6th November 2008. Liverpool, International Federation of Hydrographic Societies. 1–9.

Bell, P. S., and Osler, J. C., 2011. Mapping bathymetry using X-band marine radar data recorded from a moving vessel. Ocean dynamics 61(12), 2141-2156. DOI:10.1007/s10236-011-0478-4

Bell, P. S., Williams, J. J., Clark, S., Morris, B. D., and Vila-Concej, A., 2006. Nested radar systems for remote coastal observations. Journal of Coastal Research, Special Issue 39, 483-487.

Bell, P. S., Lawrence, J., and Norris, J. V., 2012. Determining currents from marine radar data in an extreme current environment at a tidal energy test site. In: Geoscience and Remote Sensing Symposium (IGARSS), 2012 IEEE International. 7647-7650. IEEE. DOI:10.1109/IGARSS.2012.6351856

Bell, P. S., Bird, C. O., and Plater, A. J., 2016. A temporal waterline approach to mapping intertidal areas using X-band marine radar. Coastal Engineering 107, 84-101. DOI:10.1038/NCLIMATE1944

Berry, A.J., Fahey, S., Meyers, N., 2014. Sandy beaches as dynamic refugia: Potential barriers to shoreline retreat on the Sunshine Coast, Queensland, Australia. Ocean Coast. Manag. 102, 32–39. DOI:10.1016/j.ocecoaman.2014.08.006

Blenkinsopp, C.E., Mole, M.A., Turner, I.L., Peirson, W.L., 2010. Measurements of the time-varying free-surface profile across the swah zone obtained using an industrial LIDAR. Coast. Eng. 57, 1059–1065. DOI:10.1016/j.coastaleng.2010.07.001

Bolaños, R., and Souza, A., 2010. Measuring hydrodynamics and sediment transport processes in the Dee Estuary. Earth System Science Data 2(1), 157-165.

Bolaños, R., Brown, J. M., and Souza, A., 2011. Three dimensional circulation modeling in the Dee Estuary. Journal of Coastal Research 64, 1457.

Brodie, K.L., Slocum, R.K., McNinch, J.E., 2012. New insights into the physical drivers of wave runup from a continuously operating terrestrial laser scanner, in: 2012 Oceans. IEEE, pp. 1–8. DOI:10.1109/OCEANS.2012.6404955

Castelle, B., Marieu, V., Bujan, S., Splinter, K.D., Robinet, A., Sénéchal, N., Ferreira, S., 2015. Impact of the winter 2013–2014 series of severe Western Europe storms on a double-barred sandy coast: Beach and dune erosion and megacusp embayments. Geomorphology 238, 135–148. DOI:10.1016/j.geomorph.2015.03.006

Clarke D.W., Boyle J.F., Lario J. and Plater A.J., 2014. Meso-scale Barrier Estuary Disturbance, Response and Recovery Behaviour: Evidence of system equilibrium and resilience from high-resolution particle size analysis. The Holocene 24(3), 357-369

Cowell, P.J., Thom, B.G., 1994. Morphodynamics of coastal evolution., in: Woodroffe, R.W.G., Carter, . C. D. Carter (Eds.), Coastal Evolution: Late Quaternary Shoreline Morphodynamics. Cambridge University Press, Cambridge, United Kingdom and New York, NY, USA, pp. 33–86.

Dankert, H., and Horstmann, J., 2006. A marine-radar wind sensor. In: IEEE International Symposium on Geoscience and Remote Sensing, 2006. IGARSS 2006, 1296-1299. IEEE. DOI:10.1175/JTECH2083.1

Dankert, H., Horstmann, J., and Rosenthal, W., 2003. Ocean wind fields retrieved from radar-image sequences. Journal of Geophysical Research: Oceans (1978–2012), 108(C11).

Davidson, M., Van Koningsveld, M., de Kruif, A., Rawson, J., Holman, R., Lamberti, A., Medina, R., Kroon, A., Aarninkhof, S., 2007. The CoastView project: Developing video-derived Coastal State Indicators in support of coastal zone management. Coast. Eng. 54, 463–475. DOI:10.1016/j.coastaleng.2007.01.007

Demirbilek, Z., and Sargent, F., 1999. Deep-draft coastal navigation entrance channel practice (No. CHETN-IX-1). Engineering Research and Development Center, Vicksburg MS Coastal and Hydraulics Lab.

De Vriend, H.J., Wang, Z.B., Ysebaert, T., Herman, P.M.J., Ding, P., 2011. Eco-morphological problems in the yangtze estuary and the western scheldt. Wetlands 31, 1033–1042. DOI:10.1007/s13157-011-0239-7

Dissanayake, P., Brown, J., Karunarathna, H., 2015. Impacts of storm chronology on the morphological changes of the Formby beach and dune system, UK. Nat. Hazards Earth Syst. Sci. 15, 1533–1543. DOI:10.5194/nhess-15-1533-2015

Doody, J.P., 2004. “Coastal squeeze” – an historical perspective. J. Coast. Conserv. 10, 129. DOI:10.1652/1400-0350(2004)010[0129:CSAHP]2.0.CO;2

Dugan, J.E., Hubbard, D.M., Rodil, I.F., Revell, D.L., Schroeter, S., 2008. Ecological effects of coastal armoring on sandy beaches. Mar. Ecol. 29, 160–170. DOI:10.1111/j.1439-0485.2008.00231.x

European Commission., 1999. Towards a European Integrated Coastal Zone Management (ICZM) strategy: general principles and policy options.

Flampouris, S., Seemann, J., and Ziemer, F., 2009. Sharing our experience using wave theories inversion for the determination of the local depth. In OCEANS 2009-EUROPE, 1-7. IEEE. DOI:10.1109/OCEANSE.2009.5278331

French, J., Payo, A., Murray, B., Orford, J., Eliot, M., and Cowell, P., 2015. Appropriate complexity for the prediction of coastal and estuarine geomorphic behaviour at decadal to centennial scales. Geomorphology. 256, 3-16. DOI:10.1016/j.geomorph.2015.10.005

Garcia, D., 2010. Robust smoothing of gridded data in one and higher dimensions with missing values. Computational statistics & data analysis 54(4), 1167-1178. DOI:10.1016/j.csda.2009.09.020

Gillie, R., 1997. Causes of coastal erosion in Pacific island nations. J. Coast. Res. 24, 173-204.

Hanley, M.E., Hoggart, S.P.G., Simmonds, D.J., Bichot, A., Colangelo, M.A., Bozzeda, F., Heurtefeux, H., Ondiviela, B., Ostrowski, R., Recio, M., Trude, R., Zawadzka-Kahlau, E., Thompson, R.C., 2014. Shifting sands? Coastal protection by sand banks, beaches and dunes. Coast. Eng. 87, 136–146. DOI:10.1016/j.coastaleng.2013.10.020

Hanson, H., Brampton, A., Capobianco, M., Dette, H.H., Hamm, L., Laustrup, C., Lechuga, A., Spanhoff, R., 2002. Beach nourishment projects, practices, and objectives - A European overview. Coast. Eng. 47, 81–111. DOI:10.1016/S0378-3839(02)00122-9

Hapke, C.J., Himmelstoss, E. a., Kratzmann, M., List, J.H., Thieler, E.R., 2010. National Assessment of Shoreline Change : Historical Shoreline Change along the New England and Mid-Atlantic Coasts Open-File Report 2010 – 1118. U.S. Geol. Surv. 57.

Hessner, K., Nieto-Borge, J. C., and Bell, P. S., 2008. Nautical radar measurements in Europe: applications of WaMoS II as a sensor for sea state, current and bathymetry. In Remote Sensing of the European Seas. 435-446. Springer Netherlands. DOI:10.1007/978-1-4020-6772-3_33

Heygster, G., Dannenberg, J., Notholt, J., 2010. Topographic Mapping of the German Tidal Flats Analyzing SAR Images With the Waterline Method. IEEE Trans. Geosci. Remote Sens. 48, 1019–1030. DOI:10.1109/TGRS.2009.2031843

Holland, T., Holman, R., Lippmann, T.C., Stanley, J., Plant, N., 1997. Practical use of video imagery in nearshore oceanographic field studies. IEEE J. Ocean. Eng. 22, 81–92.

Holman, R.A., Guza, R.T., 1984. Measuring run-up on a natural beach. Coast. Eng. 8, 129–140. DOI:10.1016/0378-3839(84)90008-5

Holman, R., Haller, M.C., 2013. Remote Sensing of the Nearshore. Ann. Rev. Mar. Sci. 5, 120725114348000. DOI:10.1146/annurev-marine-121211-172408

Holman, R. A., Stanley, J., 2007. The history and technical capabilities of Argus. Coast. Eng. 54, 477–491. DOI:10.1016/j.coastaleng.2007.01.003

Holman, R., Sallenger, A., Lippmann, T., Haines, J., 1993. The Application of Video Image Processing to the Study of Nearshore Processes. Oceanography 6, 78–85. DOI:10.5670/oceanog.1993.02

Holman, R., Plant, N., and Holland, T., 2013. cBathy: A robust algorithm for estimating nearshore bathymetry. Journal of Geophysical Research: Oceans 118(5), 2595-2609.

Ilić, S., Ružić, I., Ruiz de Alegria, A., 2007. Evolution of the Beach in Front of a New Seawall: Cleveleys, UK. In Coastal Structures 2007. Hrvatska znanstvena bibliografija i MZOS-Svibor.

Jessup, A.T., Zappa, C.J., Loewen, M.R., Hesany, V., 1997. Infrared remote sensing of breaking waves. Nature 385, 52–55. DOI:10.1038/385052a0

Johnson, J.M., Moore, L.J., Ells, K., Murray, a. B., Adams, P.N., MacKenzie, R. a., Jaeger, J.M., 2014. Recent shifts in coastline change and shoreline stabilization linked to storm climate change. Earth Surf. Process. Landforms 585. DOI:10.1002/esp.3650

Kirshen, P., UNH, C., UNH, M., Knuuti, K., 2014. Sea-level Rise, Storm Surges, and Extreme Precipitation in Coastal New Hampshire: Analysis of Past and Projected Future Trends.

Koopmans, B.N., Wang, Y., 1994. Satellite radar data for topographic mapping of the tidal flats in the Wadden Sea, The Netherlands., in: Proc. Second Thematic Conf. on Remote Sensing for Marine and Coastal Environments, New Orleans 31.

Kraus, N., 1988. The effects of seawalls on the beach: an extended literature review. J. Coast. Res.

Liu, Y., Li, M., Zhou, M., Yang, K., Mao, L., 2013. Quantitative Analysis of the Waterline Method for Topographical Mapping of Tidal Flats: A Case Study in the Dongsha Sandbank, China. Remote Sens. 5, 6138–6158. DOI:10.3390/rs5116138

Mancini, F., Dubbini, M., Gattelli, M., Stecchi, F., Fabbri, S., Gabbianelli, G., 2013. Using unmanned aerial vehicles (UAV) for high-resolution reconstruction of topography: The structure from motion approach on coastal environments. Remote Sens. 5, 6880–6898. DOI:10.3390/rs5126880

Marker, M., 1967. The Dee estuary: its progressive silting and salt marsh development. Trans. Inst. Br. Geogr. DOI:10.2307/621327

Mason, D., Garg, P., 2001. Morphodynamic Modelling of Intertidal Sediment Transport in Morecambe Bay. Estuar. Coast. Shelf Sci. 53, 79–92. DOI:10.1006/ecss.2000.0618

Mason, D., Davenport, I., Robinson, G.J., Flather, R.A., McCartney, B.S., 1995. Construction of an inter-tidal digital elevation model by the “Water-line” Method. Geophys. Res. Lett. 22, 3187–3190. DOI: 10.1029/95GL03168

Mason, D.C., Amin, M., Davenport, I.J., Flather, R.A., Robinson, G.J., Smith, J.A., 1999. Measurement of Recent Intertidal Sediment Transport in Morecambe Bay using the Waterline Method. Estuar. Coast. Shelf Sci. 49, 427–456. DOI:10.1006/ecss.1999.0508

Mason, D.C., Scott, T.R., Dance, S.L., 2010. Remote sensing of intertidal morphological change in Morecambe Bay, U.K., between 1991 and 2007. Estuar. Coast. Shelf Sci. 87, 487–496. DOI:10.1016/j.ecss.2010.01.015

Masselink, G., Kroon, A., and Davidson-Arnott, R. G. D., 2006. Morphodynamics of intertidal bars in wave-dominated coastal settings—a review. Geomorphology 73(1), 33-49.

Masselink, G., McCall, R., Poate, T., van Geer, P., 2014. Modelling storm response on gravel beaches using XBeach-G. Proc. ICE - Marit. Eng. 167, 173–191. DOI:10.1680/maen.14.00020

McCall, R.T., Masselink, G., Poate, T.G., Roelvink, J.A., Almeida, L.P., 2015. Modelling the morphodynamics of gravel beaches during storms with XBeach-G. Coast. Eng. DOI:10.1016/j.coastaleng.2015.06.002

McKenna, J., Cooper, A., O'Hagan, A.M., 2008. Managing by principle: A critical analysis of the European principles of Integrated Coastal Zone Management (ICZM). Mar. Policy 32, 941–955. DOI:10.1016/j.marpol.2008.02.005

Moore, R.D., Wolf, J., Souza, A.J., Flint, S.S., 2009. Morphological evolution of the Dee Estuary, Eastern Irish Sea, UK: A tidal asymmetry approach. Geomorphology 103, 588–596. DOI:10.1016/j.geomorph.2008.08.003

Nicholls, R.J., Marinova, N., Lowe, J. a, Brown, S., Vellinga, P., de Gusmão, D., Hinkel, J., Tol, R.S.J., 2011. Sea-level rise and its possible impacts given a "beyond 4°C world" in the twenty-first century. Philos. Trans. A. Math. Phys. Eng. Sci. 369, 161–81. DOI:10.1098/rsta.2010.0291

Nieto-Borge ,J. C., and Guedes Soares, C., 2000. Analysis of directional wave fields using X-band navigation radar. Coastal Engineering, 40(4), 375-391. DOI:10.1016/S0378-3839(00)00019-3.

Nieto-Borge, J. C., RodrÍguez, G. R., Hessner, K., and González, P. I., 2004. Inversion of marine radar images for surface wave analysis. Journal of Atmospheric and Oceanic Technology 21(8), 1291-1300. D DOI:10.1175/1520-0426(2004)021<1291:IOMRIF>2.0.CO;2

Nieto-Borge, J. C., Hessner, K., Jarabo-Amores, P., and de La Mata-Moya, D., 2008. Signal-to-noise ratio analysis to estimate ocean wave heights from X-band marine radar image time series. IET Radar, Sonar and Navigation 2(1), 35-41. DOI:10.1049/iet-rsn

Payo, A., Hall, J. W., French, J., Sutherland, J., van Maanen, B., Nicholls, R. J., and Reeve, D. E., 2015. Causal Loop Analysis of coastal geomorphological systems. Geomorphology 256(1), 36-48. DOI:10.1016/j.geomorph.2015.07.048

Phillips, M.R., Jones, a. L., 2006. Erosion and tourism infrastructure in the coastal zone: Problems, consequences and management. Tour. Manag. 27, 517–524. DOI:10.1016/j.tourman.2005.10.019

Plant, N. G., Holland, K. T., and Puleo, J. A., 2002. Analysis of the scale of errors in nearshore bathymetric data. Marine Geology 191(1), 71-86.

Pye, K., and Smith, A. J., 1988. Beach and dune erosion and accretion on the Sefton coast, northwest England. Journal of coastal research Special Issue 3, 33-36.

Rahman, R., and Plater, A. J., 2014. Particle-size evidence of estuary evolution: A rapid and diagnostic tool for determining the nature of recent saltmarsh accretion. Geomorphology 213, 139-152. DOI:10.1016/j.geomorph.2014.01.004

Reichert, K., Hessner, K., Nieto-Borge, J. C., and Dittmer, J., 1999. WaMoS II: A radar based wave and current monitoring system. In The Ninth International Offshore and Polar Engineering Conference. International Society of Offshore and Polar Engineers.

Roelvink, D., Reniers, A., van Dongeren, A., van Thiel de Vries, J., McCall, R., Lescinski, J., 2009. Modelling storm impacts on beaches, dunes and barrier islands. Coast. Eng. 56, 1133–1152. DOI:10.1016/j.coastaleng.2009.08.006

Rovere, A., Casella, E., Vacchi, M., Mucerino, L., Pedroncini, A., Ferrari, M., Firpo, M., 2014. Monitoring beach evolution using low-altitude aerial photogrammetry and UAV drones. Geophys. Res. Abstr. Gen. Assem. 2014 16, 1.

Ruessink, B. G., Bell, P. S., Van Enckevort, I. M. J., and Aarninkhof, S. G. J., 2002. Nearshore bar crest location quantified from time-averaged X-band radar images. Coastal Engineering 45(1), 19-32.

Ruiz de Alegria-Arzaburu, A., Masselink, G., 2010. Storm response and beach rotation on a gravel beach, Slapton Sands, U.K. Mar. Geol. 278, 77–99. DOI:10.1016/j.margeo.2010.09.004

Ryu, J., Won, J., Min, K., 2002. Waterline extraction from Landsat TM data in a tidal flat: a case study in Gomso Bay, Korea. Remote Sens. Environ. 83, 442–456. DOI:10.1016/S0034-4257(02)00059-7

Ryu, J.-H., Kim, C.-H., Lee, Y.-K., Won, J.-S., Chun, S.-S., Lee, S., 2008. Detecting the intertidal morphologic change using satellite data. Estuar. Coast. Shelf Sci. 78, 623–632. DOI:10.1016/j.ecss.2008.01.020

Santiago, I. De, Morichon, D., Abadie, S., Castelle, B., Liria, P., Epelde, I., 2013. Video monitoring nearshore sandbar morphodynamics on a partially engineered embayed beach. J. Coast. Res. Spec. Issue 458–463. DOI:10.2112/SI65-078.1

SeaZone Solutions ltd, 2015. River Dee Navigational Chart, Scale: 1:200,000. Using: EDINA Marine Digimap Service, <http://edina.ac.uk/digimap>. UK.

Senechal, N., Coco, G., Castelle, B., Marieu, V., 2015. Storm impact on the seasonal shoreline dynamics of a meso- to macrotidal open sandy beach (Biscarrosse, France). Geomorphology 228, 448–461. DOI:10.1016/j.geomorph.2014.09.025

Senet, C. M., Seemann, J., and Ziemer, F., 2001. The near-surface current velocity determined from image sequences of the sea surface. IEEE Transactions on, Geoscience and Remote Sensing 39(3), 492-505. DOI:10.1109/36.911108

Senet, C. M., Seemann, J., Flampouris, S., and Ziemer, F., 2008. Determination of bathymetric and current maps by the method DiSC based on the analysis of nautical X-band radar image sequences of the sea surface. IEEE Transactions on Geoscience and Remote Sensing 46(8), 2267-2279. DOI:10.1109/TGRS.2008.916474

Serafino, F., Lugni, C., Nieto-Borge, J. C., Zamparelli, V., and Soldovieri, F., 2010. Bathymetry determination via X-band radar data: A new strategy and numerical results. Sensors 10(7), 6522-6534. DOI:10.3390/s100706522.

Serafino, F., Ludeno, G., Flampouris, S., and Soldovieri, F., 2012. Analysis of nautical X-band radar images for the generation of bathymetric map by the NSP method. In: Geoscience and Remote Sensing Symposium (IGARSS), 2012 IEEE International, 2829-2832. IEEE. DOI 10.1109/IGARSS.2012.6350843

Sobral, F., Pereira, P., Cavalcanti, P., Guedes, R., Calliari, L., 2013. Intertidal Bathymetry Estimation Using Video Images on a Dissipative Beach. J. Coast. Res. SI 65, 1439–1444. DOI:10.2112/SI65-243.1

Stive, M.J.F., de Schipper, M. a., Luijendijk, A.P., Aarninkhof, S.G.J., van Gelder-Maas, C., van Thiel de Vries, J.S.M., de Vries, S., Henriquez, M., Marx, S., Ranasinghe, R., 2013. A New Alternative to Saving Our Beaches from Sea-Level Rise: The Sand Engine. J. Coast. Res. 290, 1001–1008. DOI:10.2112/JCOASTRES-D-13-00070.1

Takewaka, S., 2005. Measurements of shoreline positions and intertidal foreshore slopes with X-band marine radar system. Coastal Engineering Journal 47, 91-107.

Takewaka, S., Takahashi, Y., Tajima, Y., and Sato, S., 2009. Observation of morphology and flow motion at the river mouth of Tenryu with X-band radar. Proceedings of the Coastal Dynamics, Impacts of Human Activities on Dynamic Coastal Processes.

Tătui, F., Vespremeanu-Stroe, A., Preoteasa, L., 2014. Alongshore variations in beach-dune system response to major storm events on the Danube Delta coast. DOI:10.2112/SI70-117.1

Thomas, C. G., Spearman, J. R., and Turnbull, M. J., 2002. Historical morphological change in the Mersey Estuary. Continental Shelf Research 22(11), 1775-1794.

Uunk, L., Wijnberg, K.M., Morelissen, R., 2010. Automated mapping of the intertidal beach bathymetry from video images. Coast. Eng. 57, 461–469. DOI:10.1016/j.coastaleng.2009.12.002

Valenzuela, G., 1978. Theories for the interaction of electromagnetic and oceanic waves—A review. Boundary-Layer Meteorol. 13, 61–85. DOI:10.1007/BF00913863

Van Dongeren, A.R. and De Vriend, H.J., 1994. A model of morphological behaviour in tidal basins. Coastal Engineering 22(3), 287-310. DOI: 10.1016/0378-3839(94)90040

van Maanen, B., Nicholls, R., Barkwith, A., Bonaldo, D., Burningham, H., Murray, B.A., Payo, A., Sutherland, J., Thornhill, G., Townend, I.H., van der Wegen, M., 2016. Simulating mesoscale coastal evolution for decadal coastal management: A hybrid integration of multiple, complementary modelling approaches. Geomorphology 256 (68-80). DOI: 10.1016/j.geomorph.2015.10.026

Wadey, M.P., Haigh, I.D., Brown, J.M., 2014. A century of sea level data and the UK's 2013/14 storm surges: an assessment of extremes and clustering using the Newlyn tide gauge record. Ocean Sci. DOI:10.5194/os-10-1031-2014 .

Wahl, T., Jensen, J., Frank, T., Haigh, I.D., 2011. Improved estimates of mean sea level changes in the German Bight over the last 166 years. Ocean Dyn. 61, 701–715. DOI:10.1007/s10236-011-0383-x

Watanabe, Y., Mori, N., 2008. Infrared measurements of surface renewal and subsurface vortices in nearshore breaking waves. J. Geophys. Res. 113, C07015. DOI:10.1029/2006JC003950

Wengrove, M., Henriquez, M., 2013. Monitoring Morphology of the Sand Engine Leeside using ARGUS' cBathy. Coast. Dyn. 1893–1904.

Wolf, J., Brown, J. M., and Howarth, M. J., 2011. The wave climate of Liverpool Bay—observations and modelling. Ocean Dynamics, 61(5), 639-655.

Wright, L.D., Short, A.D., 1984. Morphodynamic variability of surf zones and beaches: A synthesis. Mar. Geol. 56, 93–118. DOI:10.1016/0025-3227(84)90008-2

Young, I. R., Rosenthal, W., and Ziemer, F., 1985. A three-dimensional analysis of marine radar images for the determination of ocean wave directionality and surface currents. Journal of Geophysical Research: Oceans 90(C1), 1049-1059.

List of Figures

Fig. 1. Nautical chart of the Dee estuary showing study area and maximum radar range (circle in bold) around Hilbre Island (*SeaZone Solutions Ltd*., 2015).

Fig. 2. Example time exposure image created using 256 images (~10 minutes) showing the average intensity at each pixel, a total of 336 images of this type are used in each 2-week analysis period.

Fig. 3. Schematic overview of radar waterline survey method developed by Bell et al. (2016).

Fig. 4. Radar-derived waterline elevations surveyed during April 2006 (Bell et al., 2016) showing site A, the West Hoyle sandbank and site B, the NW Wirral beach to the east of Hilbre Island. (Black rings denote areas of significant noise and line-of-sight shadowing).

Fig. 5. Comparison of (A), radar-derived waterline elevations and (B), LiDAR-observed bed elevations. (C) Residuals between (A) and (B). (D) Areas in shadow from the radar antenna defined by a simple ray-tracing method based on the LiDAR elevations, 1 = clear, 0 = shadowed.

Fig. 6. Comparison between radar-derived waterline elevations and LiDAR-observed bed elevations at West Hoyle sandbank. The 1:1 line is shown in solid green and illustrates the overestimation of elevation by the radar.

Fig. 7. (A) Estimated change in total sediment volume at site A West Hoyle sandbank. The solid line represents values estimated using the radar waterline method; the dashed line shows interpolated missing data. (C) Estimated change in sediment volume at site B NW Wirral beach. Solid line represents values estimated using the radar waterline method; dashed line the interpolated missing data; and dashed red vertical lines denote the winter seasons. (C) Wave statistics from CEFAS wavenet buoy in Liverpool Bay: daily averaged significant wave heights, daily averaged peak wave periods, and daily averaged wave directions. Red sections indicate winter seasons and red line represents monthly moving averaged values.

Fig. 8. Series of plots illustrating morphological evolution at site A, West Hoyle sandbank. Plots shown were extracted every five months between March 2006 and December 2008.

Fig. 9. Sequence of plots illustrating morphological evolution of site B, NW Wirral beach.

Fig. 10. Long-term elevation change (March 2006**–**December 2008) West Hoyle sandbank.

Fig. 11. Variation in mean waterline elevations above Chart Datum for A) site A West Hoyle sandbank and (B) site B, NW Wirral beach throughout 2006 (red line), 2007 (green line), and 2008 (blue line) around the three-year mean elevation (purple solid line).

Fig. 12. (A) Radar-estimated elevations with location of extracted section (B), extracted section rotated and the extracted cross-shore transect locations indicated.

Fig. 13. Image timestacks colour-coded by elevation. Plots show cross-shore extent along the *x*-axis, time on the *y*-axis, and elevations colour-coded. Also shown are wave energy density figures for the corresponding time periods during the survey campaign (right-hand column).

Fig. 14. (A) Radar-derived waterline elevations from the period before storm Britta (15 to 29 October). (b) Elevations from after the storm (31 October to 14 November). (c) Subimage showing radar-estimated residual waterline elevation changes (m) resulting from storm Britta (November 2006) around Hilbre Island.

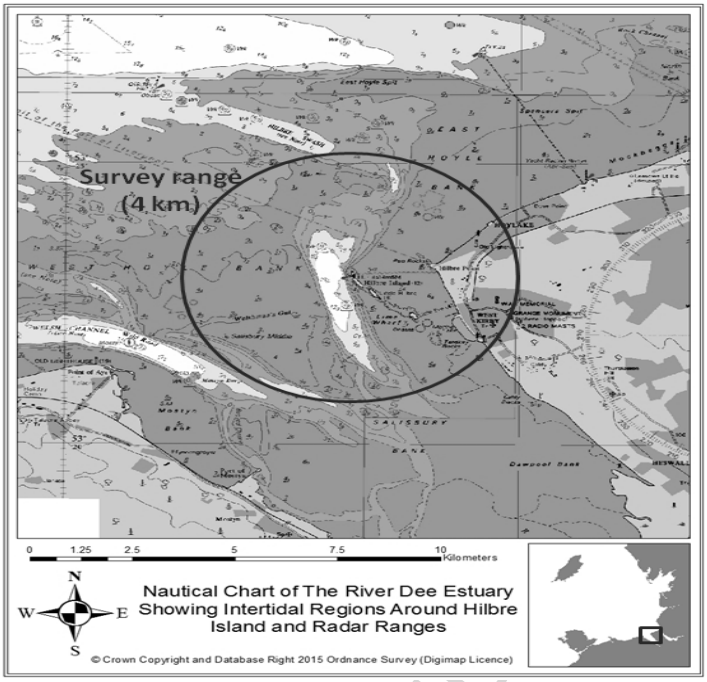

Figure 1

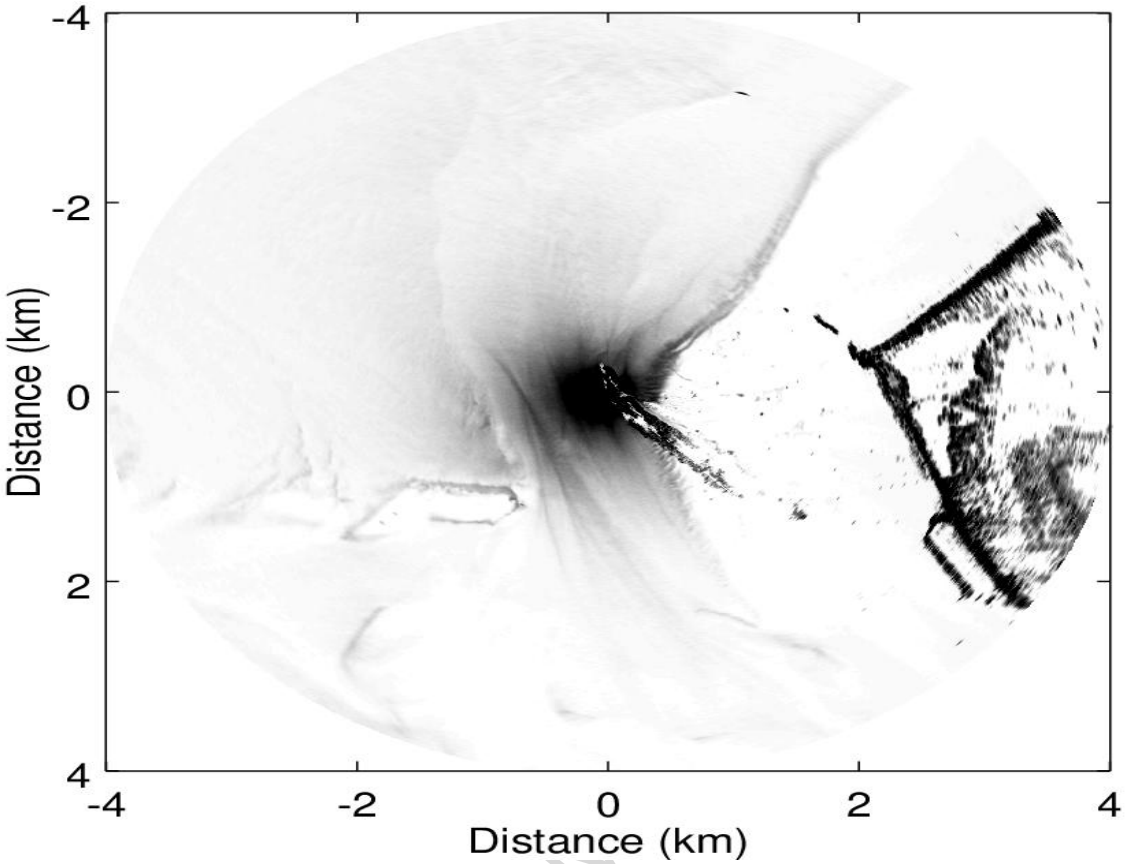

Figure 2

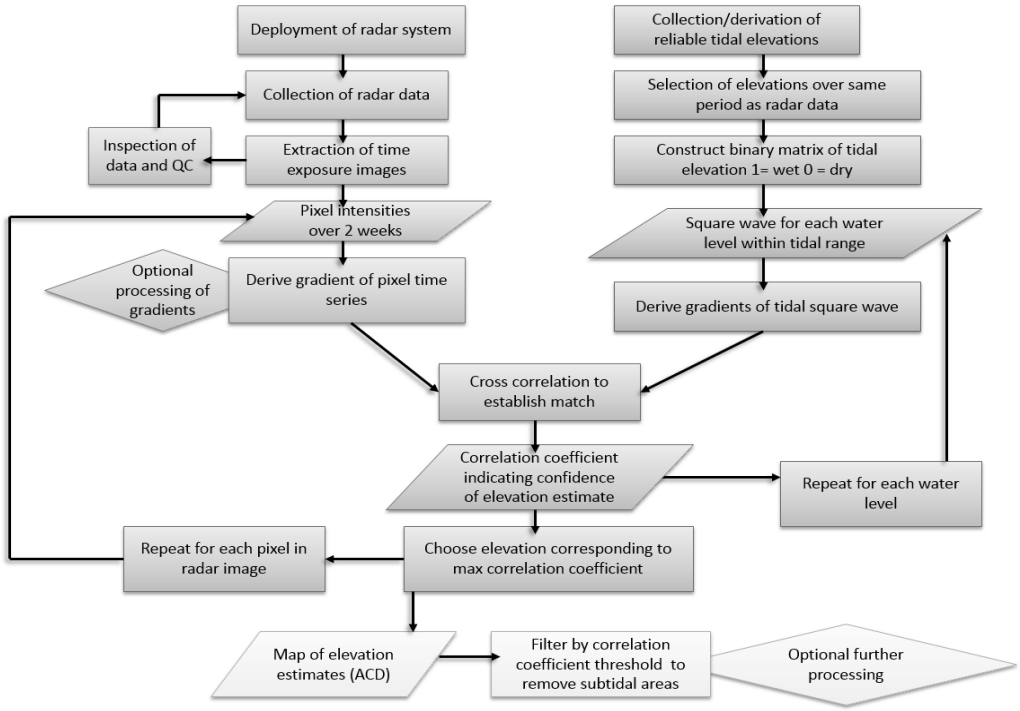

Figure 3

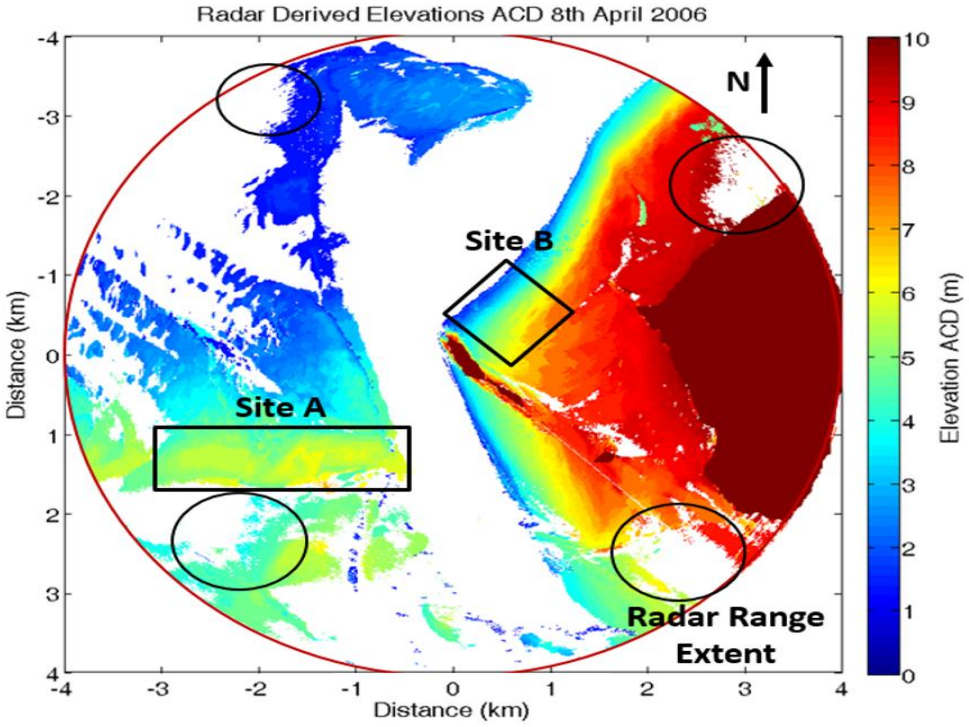

Figure 4

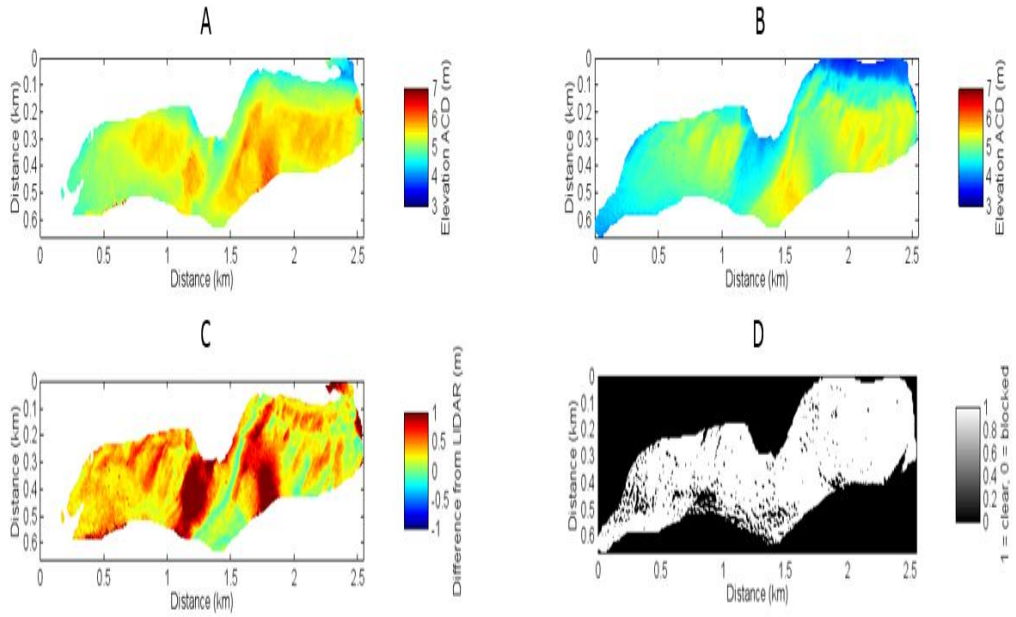

Figure 5

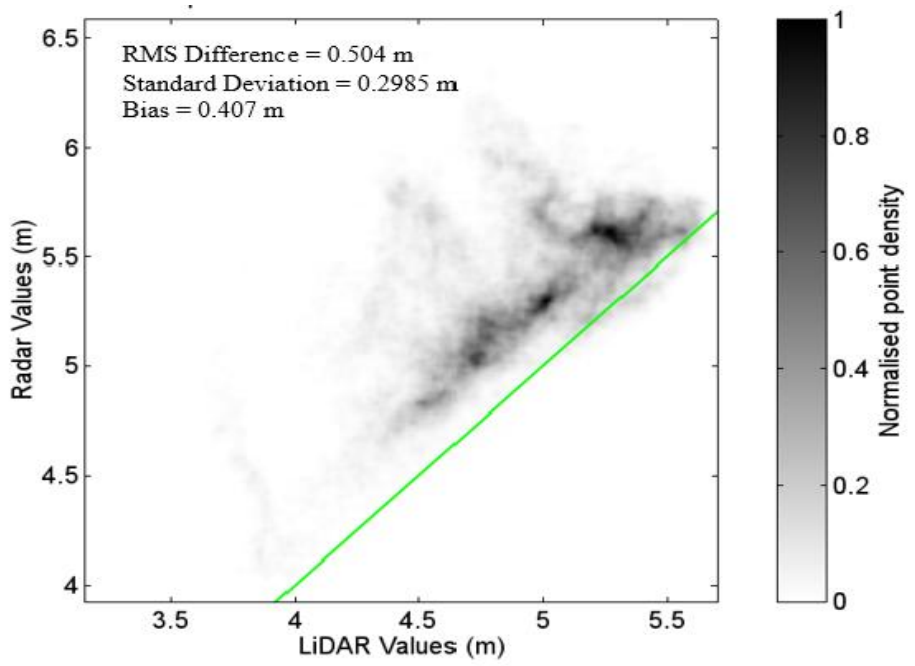

Figure 6

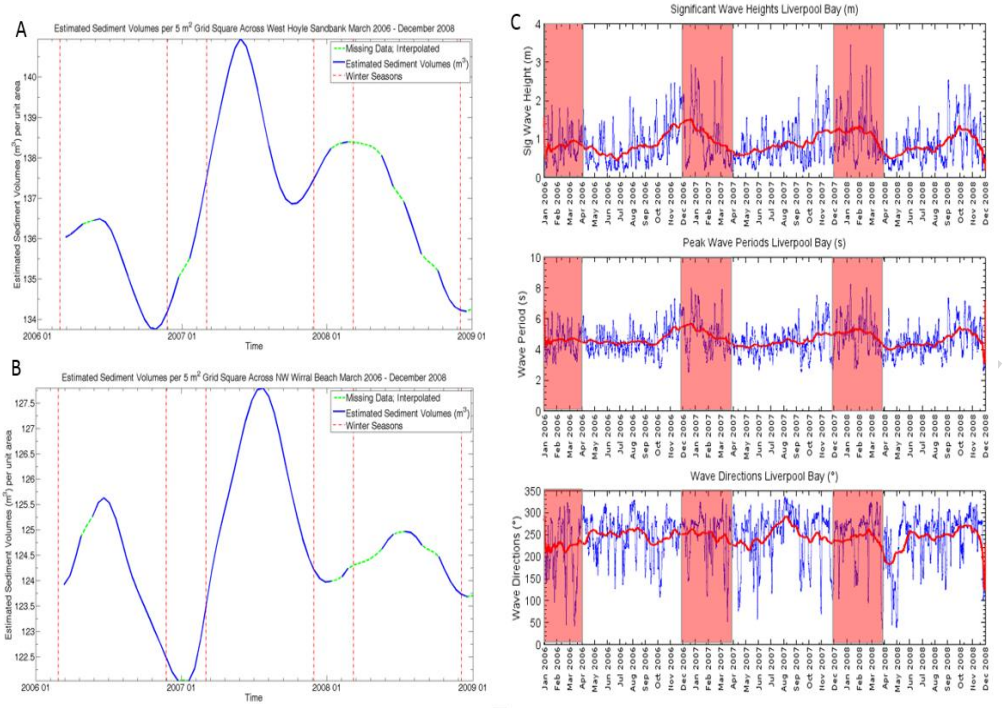

Figure 7

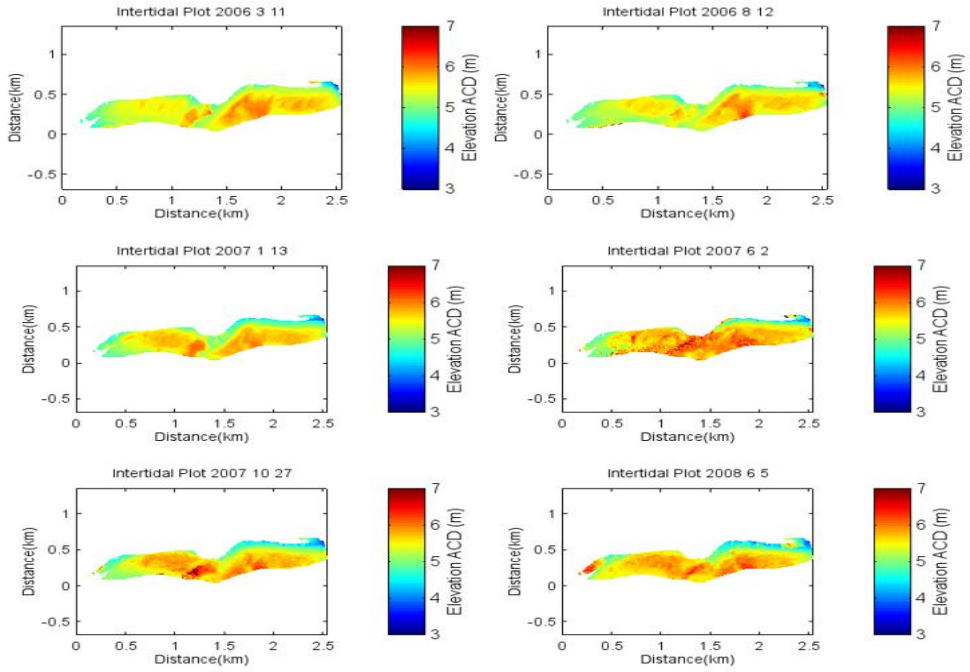

Figure 8

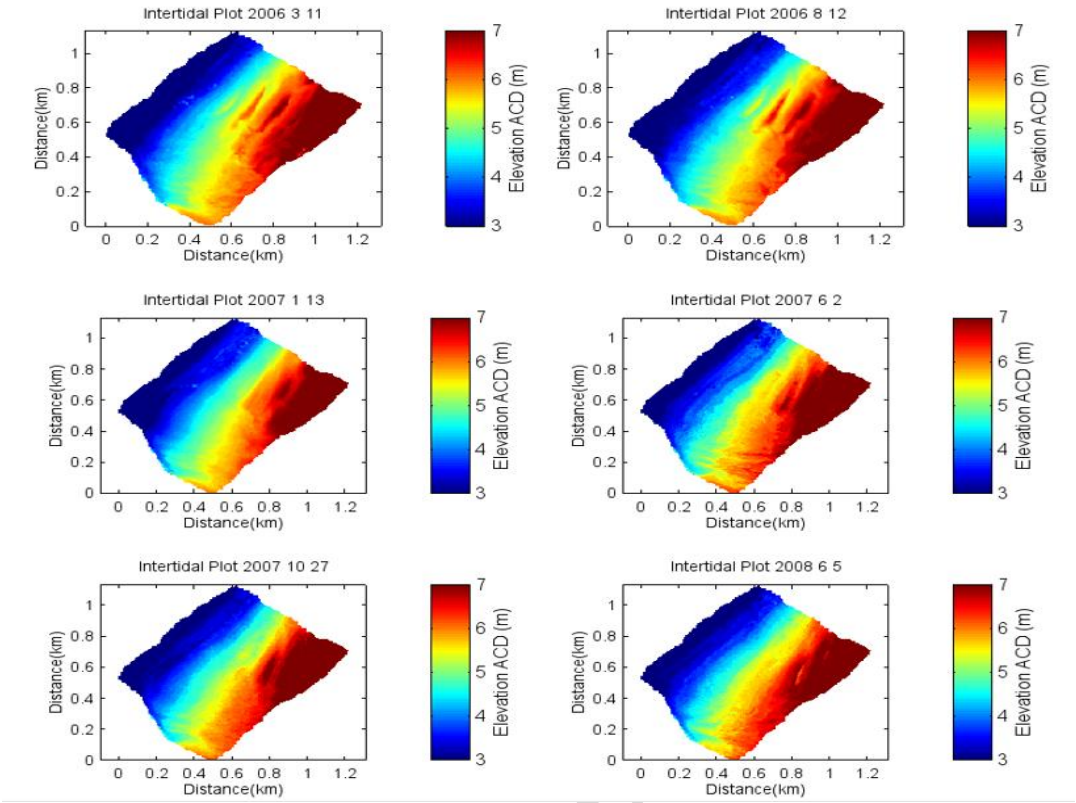

Figure 9

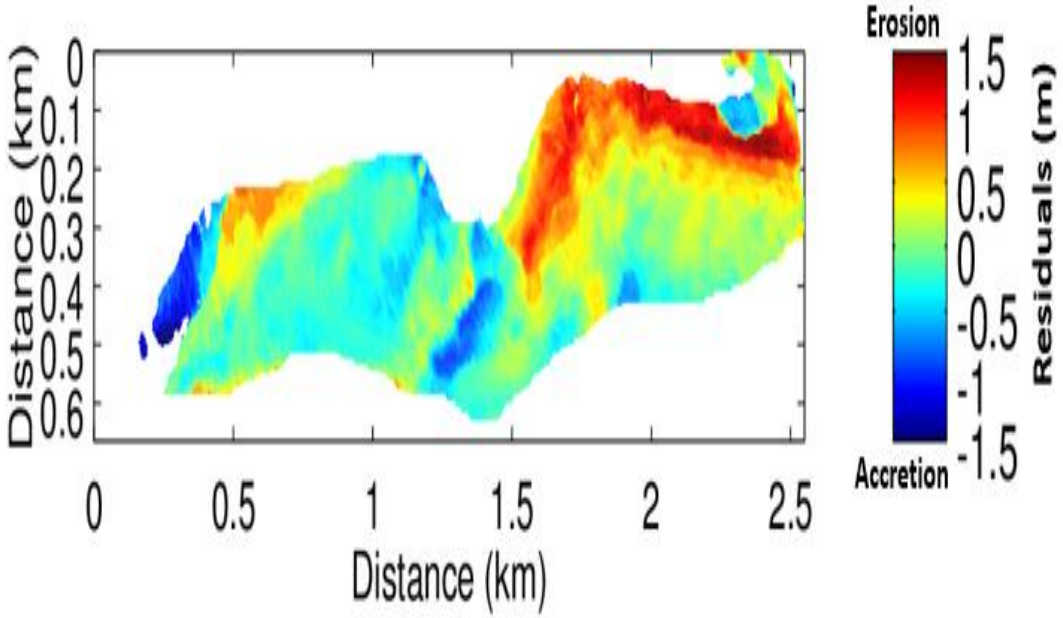

Figure 10

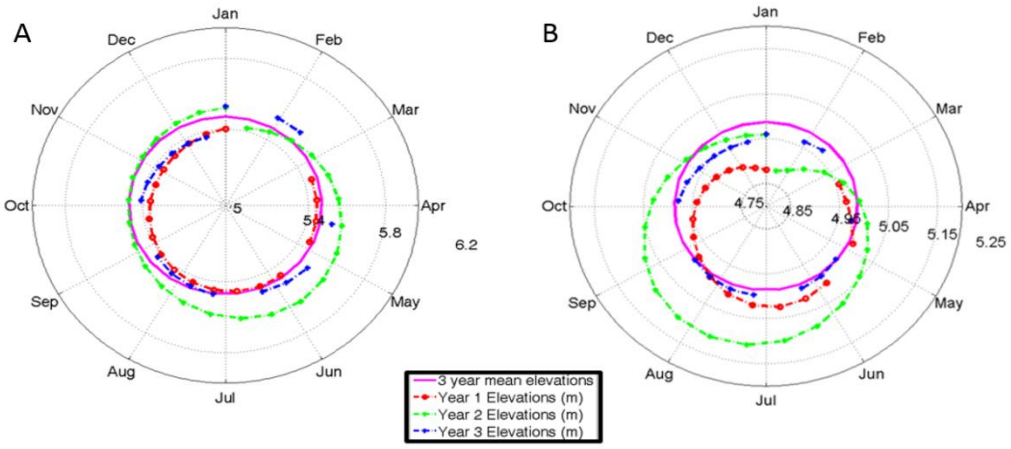

Figure 11

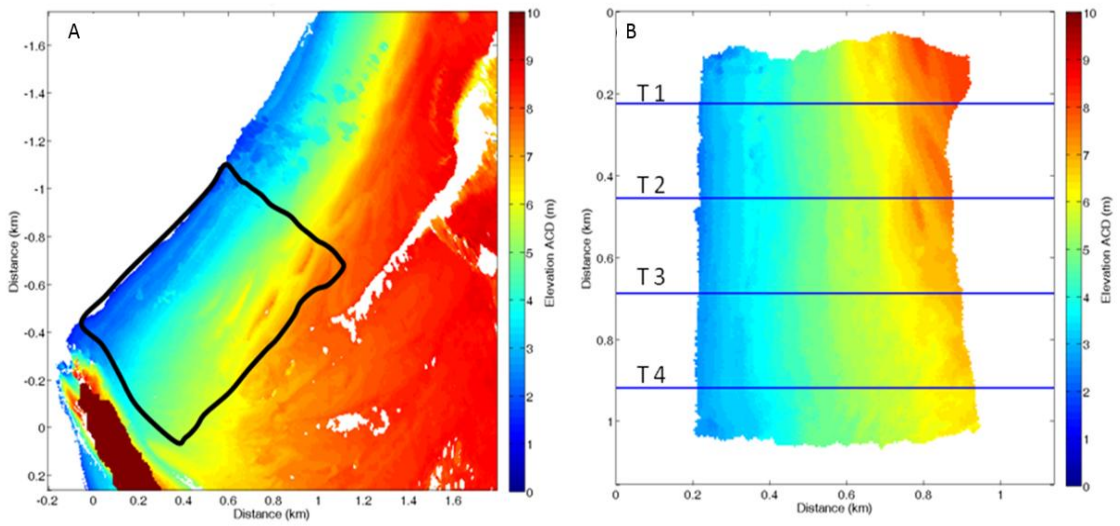

Figure 12

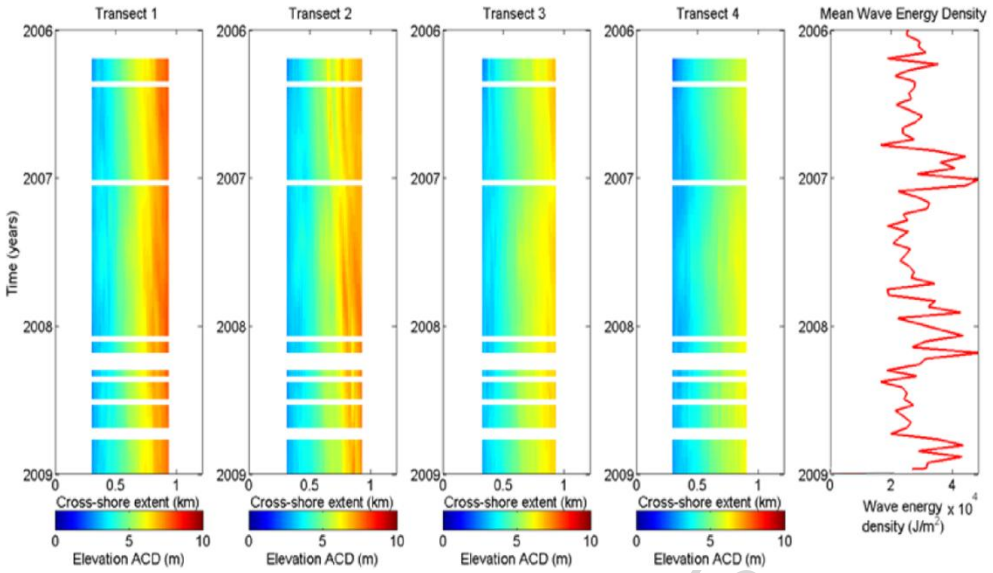

Figure 13

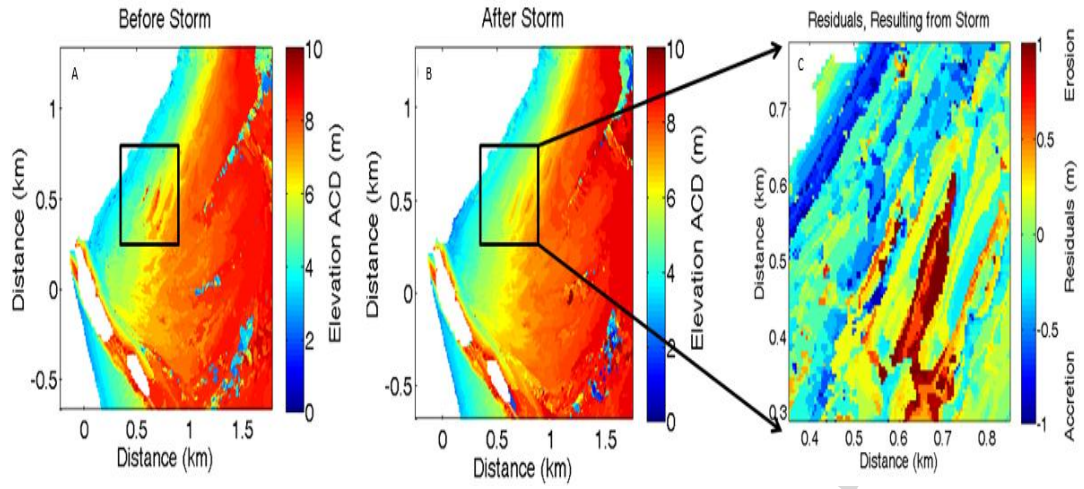

Figure 14

Highlights

- A novel radar-based remote sensing technique is applied to the task of monitoring inter- and intra-annual intertidal morphological change.
- Three years of marine radar data are analysed with a waterline mapping algorithm, generating a sequence of elevation surveys.
- Morphological evolution of the intertidal area is observed and seasonal changing sediment volumes and beach elevation trends are analysed.
- A radar waterline mapping technique is used to assess the effects of an individual storm event in 2006 on the morphology of a dissipative beach.